Atmos. Chem. Phys. Discuss., 14, 11665–11714, 2014
www.atmos-chem-phys-discuss.net/14/11665/2014/
doi:10.5194/acpd-14-11665-2014

Atmospheric Chemistry and Physics
Discussions
Open Access

Sensitivity of high-temperature weather to initial soil moisture: a case study with the WRF model

X.-M. Zeng[1,2], B. Wang[1,2], Y. Zhang[1], S. Song[1], X. Huang[1], Y. Zheng[1], C. Chen[1], and G. Wang[1,2]

[1]College of Meteorology and Oceanography, PLA University of Science and Technology, Nanjing, Jiangsu, China
[2]Key Laboratory for Mesoscale Severe Weather of Ministry of Education, Nanjing University, Nanjing, Jiangsu, China

Received: 30 December 2013 – Accepted: 22 April 2014 – Published: 9 May 2014

Correspondence to: X.-M. Zeng (zen_xm@yahoo.com)

Published by Copernicus Publications on behalf of the European Geosciences Union.

Sensitivity of high-temperature weather to initial soil moisture

X.-M. Zeng et al.

Abstract

Using the Weather Research and Forecasting model (WRF), we investigate the sensitivity of simulated short-range high-temperature weather to initial soil moisture for the East China extremely hot event in late July 2003 via a succession of 24 h simulations. The initial soil moisture (SMOIS) in the Noah land surface scheme is prescribed for five groups of designed simulations, i.e., relative to the control run (CTL), SMOIS is changed by −25, −50, +25 and +50 % in the DRY25, DRY50, WET25 and WET50 groups, respectively, with ten 24 h-long integrations performed in each group.

We focus on above-35 °C (standard of so-called "high-temperature" event in China) 2 m surface air temperature (SAT) at 06:00 UTC (roughly 12:00 LT in the study domain) to analyze the occurrence of the high-temperature event. Ten-day mean results show that the 06:00 UTC SAT (SAT06) is sensitive to the SMOIS change, i.e., SAT06 exhibits an apparent rising with the SMOIS decrease (e.g., compared with CTL, DRY25 results in a 1 °C SAT06 rising in general over land surface of East China), areas with above-35 °C SAT06 are most affected, and the simulations are found to be more sensitive to the SMOIS decrease than to the SMOIS increase, suggesting that hot weather can be amplified under low soil moisture conditions. With regard to the mechanism of influencing the extreme high SAT06, sensible heat flux shows to directly heat the lower atmosphere, latent heat flux is found to be more sensitive to the SMOIS change and results in the overall increase of surface net radiation due to the increased greenhouse effect (e.g., with the SMOIS increase of 25 % from DRY25 to CTL, the ten-day mean net radiation is increased by 5 $\mathrm{W\,m^{-2}}$), and a negative (positive) feedback is found between regional atmospheric circulation and air temperature in the lower atmosphere (mid-troposphere) due to the unique dynamic nature of the western Pacific subtropical high.

Using a method based on an analogous temperature relationship, a detailed analysis of physical processes shows that for the SAT change, the diabatic processes (e.g., surface fluxes) are affected more strongly by the SMOIS change than the adiabatic

ACPD

14, 11665–11714, 2014

Sensitivity of high-temperature weather to initial soil moisture

X.-M. Zeng et al.

process (i.e., downward airflow, or convection) in the western Pacific subtropical high in the five groups of simulations. Very interestingly, although the diabatic processes dominate over the convection process during the daytime and nighttime, respectively, they do not show to necessarily dominate during the 24 h-long periods (e.g., they are primary in the WET and CTL simulations only). It is also found that as the SMOIS decreased, the SAT06 is increased, which is largely because of the reduced cooling effect of the diabatic processes, rather than the temperature-rising effect of convection.

Unlike previous studies of heatwave events at climate time scales, this paper presents a sensitivity of simulated short-range hot weather to initial soil moisture, and emphasizes the importance of appropriate initial soil moisture in simulating the hot weather.

1 Introduction

Under the background of global warming, heat wave events have frequently occurred worldwide, especially in the early twenty-first century. As stated in a report by the World Meteorological Organization, the first decade of the century was the hottest recorded since modern measurements began around 1850 (WMO, 2013). In the summer of 2003, the Continental Europe was hit by a continuously abnormal heat wave, with the average summer temperature in most areas 3 °C higher than that from the 30 year (1961–1969) averaging, and it was estimated that there were up to 35 000 heat-related deaths across Europe (e.g., Larsen, 2003). In the same period, abnormal high-temperature weather also occurred in the regions south of the Yangtze River and South China (e.g. Lin et al., 2005; Yang and Li, 2005; Zeng et al., 2011), resulting in increased levels of daily mortality (Tan et al., 2007). In summer 2010, continuously abnormal hot weather occurred in the Eastern Europe and Russia, in which the maximum average regional temperature in the west of Russia was 8–10 °C higher than the average summer temperature for the period 2003–2009; the super heat wave events in 2003 and 2010 were likely to break the record of the maximum summer temperature of

ACPD
14, 11665–11714, 2014

the last 500 years in nearly half of the Europe (Barriopedro et al., 2011; Lau and Kim, 2012). In early July 2012, over half of the America was hit by a heat wave for about one week continuously and high-temperature records were broken in many places (Donat et al., 2013). These high temperature and heat wave events do not only directly threaten the human health and life safety, but also are easy to cause droughts and forest fires, which bring serious hazards to the whole ecological system and cause sever influence on electrical power, transportation, etc. (Tan et al., 2007; Zeng et al., 2011).

During the last decades, researchers have investigated causes for the formation and persistence of high-temperature and heat wave events in varied aspects (e.g., Wolfson et al., 1987; Lyon and Dole, 1995; Lin et al., 2005; Fischer et al., 2007; Zeng et al., 2011; Lau and Kim, 2012; among many others). Land-atmosphere interactions have been demonstrated to have an important impact on weather and climate (e.g., Shukla and Mintz, 1982; Pielke, 2001; Koster et al., 2004; Guo et al., 2011), in which the influence of soil moisture anomaly on high-temperature events has been widely investigated (Wolfson et al., 1987; Ferranti and Viterbo, 2006; Fischer et al., 2007; Fennessy and Kinter, 2011; Lau and Kim, 2012). For example, Wolfson et al. (1987) used a series of general circulation model experiments to explore the roles of sea surface temperature anomaly of the North Pacific, soil moisture anomaly of the American continent (deduced from the observed precipitation and surface temperature) and solar radiative forcing in the maintenance and weakening of the extreme heat wave of the United States in summer 1980, showing that in case of the formation of the warm and dry environment, the low soil moisture was beneficial for the maintenance of the event. As for the 2003 heat wave in Europe, Fischer et al. (2007) indicated that during the heat wave, the soil moisture was extremely low, substantially reducing latent cooling and greatly increasing the anomaly of surface temperature. Their regional climate model sensitivity simulations showed that soil moisture played a key role in the evolution of the heat wave, e.g., if there was no abnormally low soil moisture in spring, the positive surface air temperature anomaly in some areas would be reduced by about 40 %. Hirschi et al. (2011) analyzed observational indices, found a relationship between

ACPD
14, 11665–11714, 2014

soil-moisture deficit and summer hot extremes in southeastern Europe, and then compared the results with climate model simulations. Using the atmospheric general circulation model of the Center for Ocean–Land–Atmosphere Studies (COLA), Fennessy and Kinter (2011) emphasized the important roles of both the warm local sea surface temperature and the dry local soil in intensifying the 2003 European heat wave. Using two long-term WRF regional climate model simulations with and without soil moisture-atmosphere interactions to evaluate the influence of the land–atmosphere coupling on the heat wave of summer in China, Zhang and Wu (2011) found that the land–atmosphere coupling amplifies hot extremes over China, especially in most areas of eastern and southeastern China, and the increase was statistically significant. As for the summer 2010 Russian heat wave, Lau and Kim (2012) presented evidences, and demonstrated that there had been a positive feedback between the extratropical atmospheric blocking pattern and an underlying extensive land region with below-normal soil moisture, which amplified the heat wave. In most of the above-mentioned investigations, weather or climate models were used for continuous integrations for a relatively long time (e.g., seasonal) to explore the influence of soil moisture in the heat events, and it was concluded that the precedent low soil moisture or low soil moisture during the events was beneficial for the generation, maintenance or enhancement of heat waves.

Previously, there have been also many numerical studies concerning the effect on short-range weather induced by different land surface schemes or initial conditions in the models (e.g., Xue et al., 2001; Holt et al., 2006; Lei et al., 2008; Sun et al., 2012), most of which highlighted the importance of land surface processes on heavy rainfall events. However, it shows that basically there has been relatively little research focusing on the role of soil moisture in the formation or development of high-temperature weather at short time scales (e.g., 24 h). This issue is important for heat-wave research due to two aspects. Firstly, soil moisture was a key physical quantity in the land–atmosphere interaction, e.g., as described for the Global Land Atmosphere Coupling Experiment (GLACE), soil moisture-precipitation coupling strength and soil moisture

ACPD
14, 11665–11714, 2014

initialization in numerical models were respectively taken as the research focuses in the two phases of the project (Koster et al., 2006; Guo et al., 2011), in addition to above-mentioned investigations. Secondly, the role of soil moisture might differ at different timescales in affecting simulation results. In this regard, relatively long timescale soil moisture effect has received much more attention. For example, Observations have shown that in many areas, soil moisture anomalies can persist for weeks to months (e.g., Vinnikov and Yeserkepova, 1990; Seneviratne et al., 2006), and a large number of studies have quantified the effect of soil moisture initialization on the skill of subseasonal-to-seasonal climatology forecasts, showing that soil moisture anomalies or soil moisture differences did have impacts on climate variability and even substantially affected the forecast skills (e.g., Beljaars et al., 1996; Fennessy and Shukla, 1999; Viterbo and Betts, 1999; Zeng et al., 2003; Koster et al., 2004; Douville, 2010; Guo et al., 2012; among many others). As indicated by Fennessy and Shukla (1999), the strength of the impact of initial soil wetness differences was dependent on several factors, such as the areal extent and magnitude of the initial soil wetness difference, and the persistence of the soil wetness difference. In this context, the impact of initial soil wetness difference on numerical modeling with a coupled model also depends on the simulation lengths or the timescales of interest.

Therefore, with regard to short-range high-temperature weather or heat wave simulations, here naturally arise several questions in the following: (1) are the short-range (e.g., 24 h) simulations sensitive to the change in soil moisture? If yes, to what extent are they? (2) What is the mechanism responsible for the change in simulated variables (e.g., air temperature) induced by initial soil moisture? Moreover, what is the relative importance in the comparison of physical processes that affect the simulated temperature for the continental China? Answers to these questions can enhance our understanding of the influence of soil moisture and can help us improve the accuracy of high-temperature weather forecasts through better soil moisture initialization in the models.

ACPD
14, 11665–11714, 2014

The objective of this paper is to quantify and explain the sensitivity of high-temperature weather to initial soil moisture by answering the above questions. Therefore, we perform sensitivity experiments using the Weather Research and Forecasting Model (WRF) for the East China high-temperature event in late July 2003. We choose 24 h as the integration length, due to the fact that initial soil moisture is relatively less modified at this time scale of the short-range weather. Therefore, this paper is arranged as follows: in Sect. 2, the climate background of the high temperature event is described and the experimental design is given, the simulation results as well as the mechanism responsible for the soil moisture-induced temperature change are analyzed in Sect. 3, and finally Sect. 4 gives summary and discussions of the paper.

2 Methods and data

2.1 Experimental design

2.1.1 Climate background of simulation period

Previous studies have shown that the persistent strong anomalies and the exceptionally westward position of the western Pacific subtropical high were the crucial causes responsible for the continuous high temperature weather of southern China (mainly in the southeast of the continental China; see area D3 in Fig. 1a) in summer 2003 (Lin et al., 2005; Yang and Li, 2005; Zeng et al., 2011). Shown in Fig. 1b, the subtropical high in July 2003 exhibited a west-east belt distribution, spanning 15° of latitude with the westward extending ridge point of the 5880 gpm contour west of 110° E; compared to the multi-year (1971–2000) climate, both the north-south span and area of the western Pacific subtropical high were larger, the position was latitudinally over 20° westward abnormally and the intensity was stronger. In the summer East China was persistently controlled by the much stronger westward ridge of the subtropical high with weaker winds and more sunny and cloudless weather, resulting in an exceptionally hot climate.

Figure 1c and d give the anomalies of SAT and precipitation in July 2003 for the region, respectively, in which the climatologic dataset of Willmott et al. (1998) was applied. It shows that in the period, most areas south of the Yangtze River had an average SAT 1.5 °C higher than the multiyear average, while the SAT in the Huaihe River basin (30–36° N, 112–121° E) was lower than normal by 1 °C (Fig. 1c). Meanwhile, less precipitation in the regions south of the Yangtze River occurred, which is below normal by more than 2 mm d^{-1} generally and by 4 mm d^{-1} over half of the area, while there was substantially more precipitation in the Yangtze River and Huaihe River basins (Fig. 1d).

From the distribution of day-to-day SAT (not shown), the high-temperature climate with above-35 °C daily maximum SATs in southern China lasted for over one month and approximated to 2 months in some areas. Daily maximum SATs in July in the areas from the middle and lower reaches of the Yangtze River to South China were up to 38–40 °C and even reached 40–43 °C in some areas of the south-eastern coastal region, especially in late July, the hottest phase of the summer (Zeng et al., 2011). Records of the high temperature, broad area and long duration of hot weather were broken compared to the same period in history.

2.1.2 The WRF and experimental schemes

To investigate the sensitivity of model-produced high-temperature weather to initial soil moisture for the above-mentioned hot event, the Advanced Research WRF (Version 3; Skamarock et al., 2008) is employed in this study. As a community mesoscale model developed by the National Centers for Environmental Prediction (NCEP) and other research institutions, the WRF contains key dynamic features such as the fully compressible nonhydrostatic equations, complete Coriolis and curvature terms, and includes many advanced physical parameterization schemes, in which the options adopted in this study include the micro-physics scheme of Lin et al. (1983), the Betts–Miller–Janjic subgrid-scale cloud Scheme (Janjic, 1994), the Rapid Radiation Transfer Model

ACPD
14, 11665–11714, 2014

longwave radiation scheme (Mlawer et al., 1997), the Goddard shortwave radiation scheme (Chou and Suarez, 1994), the Monin–Obukhov's surface layer scheme (Hong and Pan, 1996), the YSU boundary layer parameterization scheme (Hong et al., 2006), and the Noah land surface scheme (Chen and Dudhia, 2001; Ek et al., 2003). Through the coupling between the land surface and atmospheric boundary layer schemes, the WRF accounts for land–atmosphere interactions, e.g., soil moisture-air temperature feedbacks.

Two-way nesting is used in the simulations. The simulation domain is centred at (29° N, 117.5° E), with 60 × 70 grids and a 30 km spacing for the large area D1 and 127 × 145 grids and a 10 km spacing for the small area D2 (Fig. 1a). The vertical resolution is uneven 31 layers with 50 hPa prescribed as the top of the model. In late July 2003, the extremely high temperatures mainly occurred over the areas south of the Yangtze River in eastern China (i.e., East China, denoted as area "D3" within area "D2" in Fig. 1a). Except as otherwise stated, statistical areal averages involved in the following analysis are the average values of the land part of area D3.

Similar to Zeng et al. (2011), the hottest late July is taken as the period of research in this paper. The initial fields of the simulations are selected from 06:00 UTC 20 July through 06:00 UTC 29 July 2003 (at an interval of 24 h), i.e., ten 24 h integrations are performed with a suite of model setups. In the following, each integration is labelled with the ending time of the experiment, e.g., "D21" represents the simulation with the integration period from 06:00 UTC 20 through 06:00 UTC 21 July 2003.

To investigate the sensitivity of the short-range high-temperature weather simulation to soil moisture, the initial soil moisture fields are treated as follows. Firstly, the initial field of total volumetric soil moisture content (hereafter SMOIS) is changed at each grid point, and correspondingly, the values for each soil layer are changed. Secondly, on the basis of using the analysis data to perform ten 24 h integrations (i.e., the control run or the CTL group of simulations) for late July, and following Fischer et al. (2007), sensitivity experiments are carried out with initial soil moisture modified, i.e., the four groups of simulations WET50, WET25, DRY50 and DRY25 are conducted with initial

ACPD
14, 11665–11714, 2014

moisture content changes by +50, +25, −50 and −25 % relative to CTL, respectively. In this way, the 24 h simulations for a specific date (e.g., the D21 simulation) have 5 initial fields of soil moisture, so totally 50 simulations are conducted. Meanwhile, since the SMOIS value ranges from 0 to 1 (the value of 1 presents the land cover type of inland water), in the sensitivity simulations when the first-guest value of SMOIS at a grid point is larger than the saturated one, the saturated value is then set as the initial value for integrations. Therefore, SMOIS values for inland water remain unchanged. As an example, Fig. 2 gives the surface soil moisture fields at 06:00 UTC 20 July 2003 as the initial values in the D21 simulations. Displayed in Fig. 2a, except the large inland water bodies (e.g., the Yangtze River, Taihu Lake, and Poyang Lake), soil moisture contents are generally less than 0.5 $m^3 m^{-3}$. In this case, the WET25 and WET50 soil moisture contents at the grid points can be increased by the amplitudes except for few grids that approach to saturation (Fig. 2d and e).

It should be noted that for the so-called "heat wave" events, there is no unified definition or standard. For example, the National Weather Service considers the effects of temperature and relative humidity, and an excessive heat warning is issued by the agency when daytime heat index values are expected to reach 40.5 °C or above for two consecutive days, or when they are expected to exceed 46 °C for any length of time (Kalkstein et al., 1996). While for the Euro-Mediterranean region, Stefanon et al. (2012) presented a method for defining and classifying heatwave events, in which heatwave events are classified into six classes. In China, based on climate and environmental characteristics, high-temperature weather is classified into three levels in the context of daily maximum SAT, i.e., high temperature (≥ 35 °C), harmful high temperature (≥ 38 °C), and intensely hazardous high temperature (≥ 40 °C) (Zhang et al., 2006). Because the SAT generally approaches the daily maximum value at approximately 1400 Beijing Time (i.e., 06:00 UTC) in southeastern China (especially in summer when the weather is steadily hot), following Zeng et al. (2011), we take the SAT at 06:00 UTC (SAT06) as representative of daily maximum SAT. According to observations (not shown), the above-35 °C daily maximum SAT was most manifested occurring

ACPD
14, 11665–11714, 2014

in late July 2003 over southeastern China. In the context of the high-temperature classification in China, to investigate the sensitivity of simulated hot weather to initial soil moisture, we therefore focus on SAT06 results and related quantities for the study period of late July 2003, with an integration length of 24 h for each simulation.

2.2 The data

The meteorological initial and lateral boundary conditions for the WRF model, including the data of soil moisture for CTL, are derived from NCEP Final (FNL) Operational Global Analysis data that are on 1° by 1° grids prepared operationally every six hours (00:00, 06:00, 12:00 and 18:00 UTC; http://rda.ucar.edu/datasets/ds083.2/). The FNL analysis data are from the Global Data Assimilation System that continuously collects observational data for many analyses, and are made with the same model in the NCEP Global Forecast System (GFS), a global spectral data assimilation and forecast model system (e.g., Whitaker et al., 2008). The data are prepared about an hour or so after the GFS is initialized because such a delay facilitates the use of more observational data. The GFS also uses the FNL data from the previous 6 h cycle as part of its initialization. Besides, WRF is also recommended to use the dataset as an option for mesoscale weather simulations (http://www.dtcenter.org/wrf-nmm/users/downloads/input_data.php).

For validation of the temperature (i.e., SAT06) simulations, conventional observational data from the meteorological stations are used. Shown in Fig. 1a, there are 369 stations in the core region of East China for the assessment.

2.3 Analysis of physical processes

We mainly focus on the change in air temperature due to the modified SMOIS. The temporal change in air temperature is governed by the partial differential equation which is

ACPD
14, 11665–11714, 2014

derived from the first law of thermodynamics, i.e.,

$$\frac{\partial T}{\partial t} = -\boldsymbol{V} \cdot \nabla T - w(\gamma_\mathrm{d} - \gamma) + H_t, \tag{1}$$

where $\boldsymbol{V}$ represents the horizontal wind vector, w the vertical velocity, γ_d and γ the atmospheric temperature lapse rate and the dry adiabatic lapse rate, respectively, and H_t the diabatic heating term. We let

$$T_\mathrm{t} = \int_t \frac{\partial T}{\partial t} \mathrm{d}t,$$

$$\mathrm{ADV} = -\int_t V \cdot \nabla T \, \mathrm{d}t,$$

$$\mathrm{CON} = -\int_t w(\gamma_\mathrm{d} - \gamma) \mathrm{d}t,$$

and

$$Q_\mathrm{t} = \int_t H_\mathrm{t} \mathrm{d}t$$

represent integral terms for local temperature change, advection and convection effects, and diabatic effect, respectively, and then Eq. (1) can be rewritten as

$$T_\mathrm{t} = \mathrm{ADV} + \mathrm{CON} + Q_\mathrm{t}. \tag{2}$$

It indicates that there are three factors (terms; units are in Kelvin) influencing T_t on the right hand side of Eq. (2): the first term, ADV, means that warm (cold) advection causes the increase (decrease) of local temperature; the second term, CON, suggests that under stable stratification ($\gamma_\mathrm{d} - \gamma > 0$), ascending (descending) motion results in adiabatic cooling (warming) in the lower atmosphere, while the situation is opposite under unstable stratification ($\gamma_d - \gamma < 0$); the third term, Q_t, includes diabatic influence from radiation, turbulent exchange and condensation processes, etc. Except Q_t, the other three terms of Eq. (2) can be calculated by the simulation outputs, and therefore Q_t can be obtained. In this way, the relative contributions of the factors to air temperature change can also be examined.

Because there are few 2 m meteorological quantities in the model outputs, it is unlikely to directly calculate all the terms in Eq. (2). Therefore, we utilize the analogous relationship between air temperature at 2 m and that at the lowest model level where model outputs are adequate (see Sect. 3.2.4), and explain to what extent 2 m temperature is affected by the physical processes.

3 Results and discussion

3.1 Quantifying the sensitivity: preliminary results of temperature

Because all the model settings and boundary and initial conditions except the initial soil moisture contents are the same in the simulations, differences between the simulations are caused by different initial soil moisture contents. In addition, to examine the overall influence of different initial soil moisture contents on the short-range high-temperature simulations for late July 2003, following Xue et al. (2001) and Zeng et al. (2011), we use the ten-day means of simulated results in the following sections, in a large part, to investigate the event climatologically and systematically. Therefore, in this section we analyze preliminarily the soil moisture-induced differences in ten-day mean SAT06 in the simulations.

3.1.1 Spatial distribution

As addressed above, spatial SAT06 distributions mean, approximately, the maximum SAT values over East China, and the occurrence of the hottest weather during the study

ACPD
14, 11665–11714, 2014

period. Figure 3 gives average distributions of ten-day mean SAT06 for the simulations, showing that the central position, range and strength of high temperature simulated in the CTL run (Fig. 3b) are basically consistent with those in the NCEP FNL analysis field (Fig. 3a), i.e., the areas with above-35 °C SATs are located between 26–32° N (the central part of the study continental area), and the central position of high values is well simulated. Nevertheless, the simulated high-temperature (above 35 °C) area is slightly larger and a little northward compared to the analysis data.

Compared with CTL, changing initial soil moisture can substantially change the simulation results. For instance, in contrast with CTL (Fig. 3b), the central positions of high temperature of SAT06 in DRY25 (Fig. 3c) and DRY50 (Fig. 3d) remain basically unchanged, but the range and intensity of simulated high temperature are apparently enlarged and strengthened; CTL gives a simulated maximum temperature of around 37 °C with a relatively small area higher than the value, while the maximum DRY25 temperature is higher than 38 °C (i.e., harmful high temperature) with a large total area of above 37 °C covering most of the CTL areas of above 35 °C, and the maximum temperature of DRY50 exceeds 40 °C and the harmful high temperature almost covers the area north of 26° N. It clearly shows that with the decreasing of SMOIS, the simulated SAT06 rises. Also compared with CTL (Fig. 3b), the high temperature ranges in WET25 (Fig. 3e) and WET50 (Fig. 3f) are obviously decreased and the intensities are weakened, i.e., WET25 produces a maximum temperature of ~ 36 °C, with a much less area for above-35 °C SAT06, and WET50 only gives a maximum of ~ 35 °C with a very small area coverage for above-35 °C SAT06 which shows almost no high temperature simulated in the entire domain. In previous climate studies, regions with intermediate soil moisture have been found to be sensitive to soil moisture-precipitation coupling (e.g., Koster et al., 2004). Based on regional climate model simulations for the 2003 European heat wave, Fischer et al. (2007) suggested that the soil moisture sensitivity was low at dry (near wilting point; e.g., DRY50 in their simulations) and at wet (near field capacity; e.g., WET50) soil moisture contents and was strong at the intermediate contents. Unlike Fischer et al. (2007), we adopt the WRF for short-range weather

ACPD
14, 11665–11714, 2014

simulations, despite the further change in SMOIS, it is unable to be close to the wilting point or field capacity overall for the study domain within 24 h (i.e., total soil moisture is less changed at the short time scale compared to long-period climate simulations with persistent prolonged changing of soil moisture in heat wave events; see Sect. 3.2 for soil moisture variations), and therefore the SMOIS-induced sensitivity is high at least for the heat wave development in the short range, i.e., the above results suggest that with the SMOIS increase, the simulated SAT06 is decreased evidently, even in some dry or wet soil moisture conditions. Meanwhile, with the SMOIS change, the SAT in the lower troposphere (e.g., 850 hPa) presents a change similar to SAT06 (not shown). All these results show that the high-temperature simulations with a short-term (24 h) integration length are very sensitive to the change in initial soil moisture.

To have a closer look at the influence of the SMOIS change, further comparisons are made between CTL and the sensitivity simulations (Fig. 3g–j). Compared with CTL, DRY25 presents a SAT06 rise by more than 1 °C over most of the land areas (Fig. 3g), while the SAT06 in DRY50 rises more than 2 °C generally and 4 °C maximally over land (Fig. 3h). On the contrary, WET25 reduces the temperature in most areas by above 0.5 °C (Fig. 3i), while WET50 does so by more than 1 °C with a maximum decreasing higher than 2 °C (Fig. 3j). For a given sensitivity simulation, the amplitude of temperature rising (decreasing) differs in different areas, which is closely related with the forcings of surface energy balance, such as sensible and latent heat fluxes, in the areas (see Sect. 3.2). By comparing the four groups of sensitivity simulations with CTL, it is found that the magnitude of temperature rising of DRY50 (DRY25) is more than that caused by WET50 (WET25), suggesting that the higher sensitivity of simulated SAT06 is induced by lower soil moisture. In addition, the area with the largest SAT06 change is found to lie over/around the area with above-35 °C high temperatures. All these indicate that the change in initial soil moisture has a very large influence on the SAT06 simulation, or in other words, on the development of short-range (24 h) extremely high temperature weather.

ACPD
14, 11665–11714, 2014

Figure 4 gives the average SAT06 values for area D3 in the simulations. In agreement with the above results, higher soil moisture simulations produce lower area-averaged SAT06 for each simulation (Fig. 4a). It is worth noting that as SMOIS reduced from by 25 to by 50 %, relative to CTL, the magnitude of the SAT06 increase (i.e., between DRY25 and DRY50) is larger than that of the decrease when SMOIS is increased from by 25 to by 50 % (i.e., between WET25 and WET50). This result is consistent with a conclusion in previous climate studies (e.g., Fischer et al., 2007; Zhang and Wu, 2011), i.e., because low soil moisture strongly reduced latent cooling, the surface temperature anomalies or heat waves were amplified. Our results show that during the 24 h integrations, the high temperature simulation is more sensitive to the decrease of soil moisture than to the increase. The reason for the results is straightforward: lower thermal inertia induced by lower soil moisture leads to higher temperature, under given energy forcings. Figure 4b further gives the nonlinear change result of the ten-day mean SAT06 in area D3 for the five groups of simulations, showing a nonlinear SAT06 change, with the WET25 – WET50, CTL – WET25, DRY25 – CTL and DRY50 – DRY25 differences of 0.44, 0.73, 0.92 and 1.48 °C, respectively. All these further confirm that high-temperature short-range weather simulations are very sensitive to the decrease of initial soil moisture.

3.1.2 Simulation errors

In order to examine the consistency of simulations with observations and to access the sensitivity results under different soil moisture conditions, the simulation results are interpolated to meteorological stations (Fig. 1a). In the following, the model bias (BIAS) and root-mean-square error (RMSE) are applied, which are computed as

$$\mathrm{BIAS} = \overline{M} - \overline{O}, \tag{3}$$

$$\mathrm{RMSE} = \sqrt{\frac{1}{N}\sum_{i=1}^{N}(M_i - O_i)^2}, \tag{4}$$

ACPD
14, 11665–11714, 2014

Sensitivity of high-temperature weather to initial soil moisture

X.-M. Zeng et al.

where M is the simulated quantity, and O is the observation.

Figure 5 gives the BIAS and RMSE values for SAT06 in each simulation. The CTL run shows to give a SAT06 value most approximate to the observation, with the ten-day mean SAT06 value 0.14 °C lower than the observation (Fig. 5a), suggesting that the BIAS in each sensitivity simulation is generally consistent with the SAT06 difference between the simulation and CTL. The ten-day mean SAT06 values of DRY50 and DRY25 are respectively 2.5 and 0.90 °C higher than the observation, with a relative difference exceeding 150 % (relative to DRY25), while the SAT06 values of WET50 and WET25 are respectively 1.5 and 0.96 °C lower, with a difference up to 50 % (relative to WET25). These day-to-day results further demonstrate that the high-temperature weather simulation is very sensitive to the change in soil moisture and is more sensitive at a lower level of soil moisture than at a higher level, or in other words, the hot weather can be amplified under low soil moisture conditions. Similar results can be seen from RMSE values (Fig. 5b), e.g., the average RMSE values of DRY50 and DRY25 amount to 3.9 and 3.0 °C, respectively, showing a quite large difference.

3.2 Explanation of the sensitivity: details of physical processes

In the context of the mechanism responsible for the sensitivity, the SAT difference induced by initial soil moisture is directly caused by different land surface energy fluxes, and by modified regional dynamic circulation as well. Among the fluxes, upward sensible heat transfer directly heats the low-level atmosphere and plays a key role in influencing the SAT, while latent heat flux is modified by the change in soil moisture, directly changes with evaporation, and further affects the SAT, e.g., decreased soil moisture leads to lower evaporation which reduces the cooling effect of the land surface, and results in higher sensible heat flux to heat the lower troposphere.

ACPD
14, 11665–11714, 2014

3.2.1 Soil moisture

The Noah land surface scheme calculates the soil moisture for four layers with thickness of 10, 30, 60 and 100 cm for the L1, L2, L3 and L4 layers, respectively. Figure 6 shows the variations of the ten-day mean soil moisture in the five groups of simulations. On the whole, changes in soil moisture within 24 h are closely related to the depths of soil layer and initial values of soil moisture. The shallow soil moisture is changed significantly, while the deep soil moisture is less modified and even remains almost unchanged. Shown in Fig. 6a, the CTL soil moistures of L3 and L4 are changed a little, while those of L1 and L2 are decreased more evidently due to continuous evaporating, which is consistent with the late July weather with more sunny days and no rainfalls. In DRY25 the surface soil moisture shows to be recharged by the lower soil layer because the surface moisture is very low (lower than that in CTL which is "normally" dry), and the surface soil moisture after 24 h is still almost unchanged (Fig. 6b); similar is the DRY50 surface soil moisture, yet with a temporal increase (Fig. 6c). Results of WET25 and WET50 are contrary to those of the DRY simulations, in which shallow soil moisture of the former is changed significantly due to too adequate water supply under the dry, hot weather and the model shows to spin up with $\sim 10\,\%$ decreases of surface moisture during the first hour of integrations (Fig. 6d and e). These spin-up behaviors highlight that initial soil moisture values should be appropriately applied to specific models in response to model configurations.

3.2.2 Sensible and latent heat fluxes

Figure 7 shows ten-day mean spatial distribution of 06:00 UTC sensible heat flux of the simulations. Comparing Fig. 7b–e with Fig. 3g–j, the high-value area of sensible heat flux difference corresponds very well with that of high-temperature difference and is also consistent with the above-35 °C high-temperature central area, which shows that the decrease (increase) of initial soil moisture causes the increase (decrease) of sensible heat flux, thus directly leads the temperature rise (drop). These results

ACPD
14, 11665–11714, 2014

indicate that sensible heat flux is a key factor for simulated SAT06 in the simulations, as is consistent with conclusions given in previous studies, e.g., the soil moisture-temperature coupling is mainly determined by the ability of the soil moisture to affect surface fluxes (e.g., Fischer et al., 2007; Zhang et al., 2011). Meanwhile, it also shows that similar to long-term (e.g., three-month-long) climate simulations, the short-range (24 h) simulations with different soil moistures can cause changes in surface fluxes which further affect and well respond to simulated SAT results.

Corresponding to Fig. 7, Fig. 8 displays the simulated 06:00 UTC latent heat fluxes. In comparison of Fig. 8b–e with Fig. 7b–e, it is found that the area of small latent heat flux differences also well agrees with the area of large sensible heat flux differences and meanwhile is also consistent with the high value area of SAT06 differences (Fig. 3g–j). The reason is that surface latent heat flux and sensible heat flux are different distribution forms partitioning net radiation; under the circumstance of stable net radiative energy at a specific time point, the decrease (increase) of latent heat flux would lead to the increase (decrease) of sensible heat flux, and thus induce the rising (dropping) of low-level temperatures. In addition to the land surface changes, different SMIOS values which cause the change in surface latent heat flux would also, indirectly by modifying the radiative forcing and circulation of the atmosphere, lead to change in the SAT (addressed at the end of this subsection).

Figure 9 shows hourly variations of ten-day mean surface quantities, showing that the simulated sensible and latent heat fluxes and the SAT are sensitive to the changes in initial soil moisture and the response is very fast with pronounced differences after one hour of integration. Because the surface sensible heat and latent heat are two of the main forms partitioning net radiation, the change in soil moisture can directly cause the difference in partitioning of net radiation into sensible and latent heat fluxes at a given time. Comparing Fig. 9a with b shows that the simulated sensible heat fluxes of the DRY simulations are higher than that of CTL while the latent heat fluxes are lower, whereas contrary results are shown in the WET simulations. Additionally, the lower (or higher) the initial value of soil moisture is, the higher (or lower) the corresponding

ACPD
14, 11665–11714, 2014

simulated sensible heat flux is and the lower (or higher) the simulated latent heat flux is, leading to higher (or lower) SAT (Fig. 9c). At night, the simulated sensible and latent heat fluxes show little differences between different simulations, but due to the accumulative effect of energy transmission, the daytime SMOIS-induced effect adds to nighttime temperatures, thus the nighttime SAT still shows clear differences; after sunrise, the sensible heat and latent heat are increased fast and reach their peak values at 04:00 UTC, while the SATs reach the maxima at 06:00 UTC, showing the changes in sensible and latent heat fluxes is anterior to the SAT change, which is also consistent with many observations in the planetary boundary layer (e.g., Liu et al., 2011).

Figure 10 presents sensible and latent heat fluxes for 06:00 UTC in the D21–D30 simulations as well as the flux and SAT06 differences between the sensitivity simulations and CTL. Similar to the above results, the sensible and latent heat fluxes show to be sensitive to the change in SMOIS, and the DRY sensible heat flux is larger while the latent heat flux is smaller compared to CTL. In addition, sensible and latent heat fluxes and the temperature are more sensitive to the decrease of soil moisture, i.e., amplitudes of the DRY25 – CTL and DRY50 – DRY25 flux differences are larger than those of the CTL – WET25 and WET25 – WET50 differences, respectively, e.g., the DRY50 – DRY25 sensible heat flux difference is 67 $\mathrm{W\,m^{-2}}$ larger than the WET50 – WET25 difference (Fig. 10a), and corresponds to a latent heat flux difference of about 85 $\mathrm{W\,m^{-2}}$ (Fig. 10b) and an SAT06 difference of about 1.6 °C. Meanwhile, features of the ten-day mean quantities at 06:00 UTC are consistent with those of the ten-day means averaged with hourly values (e.g., the sensible heat fluxes in Fig. 10a vs. Fig. 10c), suggesting that the high-temperature differences for 06:00 UTC (i.e., differences in above-35 °C SAT06) are caused by the SMOIS-induced persistent forcings during the 24 h.

Shown in Fig. 10d, high (low) average sensible heat flux well corresponds to high (low) SAT06, and low (high) latent heat flux is closely associated with high (low) SAT06, indicating that the SMOIS decrease (increase) leads to decreased (enhanced) surface evaporation or latent heat flux. It is worth noting that while the SMOIS change

ACPD
14, 11665–11714, 2014

is nonlinearly related with the change in 24 h-averaged sensible heat flux, the change in the sensible heat flux basically corresponds to the SAT06 change with an approximately linear relationship. Further inspection in the context of relative differences (represented in percentage) indicates that compared to latent heat flux, the change in sensible heat flux is more affected by soil moisture, e.g., relative to CTL, the difference between WET50 (DRY50) and CTL is 16.4 % (−40.0 %) in latent heat flux and −49.6 % (139.6 %) in sensible heat flux. Theoretically, sensible heat flux has a direct influence on SAT, and the above results further demonstrate the substantial effect of sensible heat flux on SAT06, i.e., on the development of the 24 h high temperatures.

In addition, as the SMOIS changes, the modified latent heat flux also has more significant and complex implications for surface energy balance. Table 1 lists the ten-day mean 06:00 UTC values and those averaged with hourly outputs for surface quantities in the five groups of simulations. What is interesting is that the variation of soil moisture can bring about the variation of net radiation and therefore lead to apparent differences between the amplitude of the change in sensible heat flux and that in latent heat flux, i.e., the SMOIS increase (decrease) results in the larger increase (decrease) amplitude of latent heat flux than the decrease (increase) amplitude of sensible heat flux, which leads to the increases (decreases) of the surface net radiation. For example, the CTL daily average Bowen ratio (ratio of sensible heat to latent heat) is about 0.2; as soil moisture decreased, Bowen ratio is increased correspondingly with 24 h means of about 0.3 and 0.8 in DRY25 and DRY50, respectively, and owing to the increase of sensible heat flux, the SAT rises. Results of ten-day mean quantities at 06:00 UTC are similar to those from hourly values, showing that the surface net radiation is increased with soil moisture and results in the increase of the sum of the sensible and latent heat fluxes. As reported by previous studies (e.g., Baldocchi et al., 2001), Bowen ratio of well-vegetated humid areas is generally less than 1; therefore latent heat flux, other than sensible heat flux, is the primary form partitioning net radiation at the land surface. Due to the SMOIS increase, latent heat flux (i.e., water vapor flux) is increased much more, which produces stronger greenhouse effect and strengthens the

Title Page
Abstract Introduction
Conclusions References
Tables Figures
◂ ▸
Back Close
Full Screen / Esc
Printer-friendly Version
Interactive Discussion

downward atmospheric longwave radiation. Meanwhile, because sunny weather persisted during the simulation period, little was the change in clouds-induced reflected solar radiation and the SMOIS-induced effect of added water evaporation on shortwave radiation is suggested to be also small, thus the surface net radiative energy is largely increased with the greenhouse effect of water vapor. For instance, as SMOIS is increased by 25 % from DRY25 to CTL, ten-day mean net radiation from hourly values is increased by about 5 $\mathrm{W\,m^{-2}}$, which shows to be quite large as compared to the sensitivity of regional suface net radiation to deforestation in the Amazon Basin at a scale of $10^6\,\mathrm{km}^2$ (Dickinson and Kennedy, 1992); also, the 06:00 UTC net radiation is increased by about 12 $\mathrm{W\,m^{-2}}$, and the sums of sensible heat and latent heat fluxes are increased by similar amplitudes. However, due to the SMOIS increase, the added net radiation is still less than the decrease of the sums, which is induced by increased ground heat flux, and therefore the overall effect of the SMOIS increase shows a cooling at the land surface, e.g., the CTL ten-day mean SAT06 is about 1 °C lower than that of DRY25.

3.2.3 Atmospheric circulation

The SAT variation is closely related with changes in regional atmospheric circulation which is one of the key elements of synoptic system over the region. Figures 11 and 12 respectively show the 500 and 850 hPa geopotential height fields and their differences caused by the SMOIS change. As stated in Sect. 2, the western Pacific subtropical high is the crucial regime controlling the weather over continental China in summer. This indicates that the drop (rise) of geopotential height at a given pressure level means the weakening (intensifying) of the subtropic-high atmospheric circulation. Shown in Figs. 11a and 12a, the weather during late July 2003 was controlled by the subtropical high and the SMOIS decrease (increase) leads to strengthening (weakening) of the 500 hPa (850 hPa) geopotential height. For example, compared to CTL, the DRY50 500 hPa geopotential height in the simulated area is generally increased by over 2 gpm with a maximum value over 4 gpm (Fig. 11c); the soil moisture-induced effect on the 850 hPa geopotential height is contrary to that at 500 hPa, i.e., the SMOIS decrease

ACPD
14, 11665–11714, 2014

Sensitivity of high-temperature weather to initial soil moisture

X.-M. Zeng et al.

(increase) leads to the enhancement (reduction) of the 850 hPa geopotential height in most of the simulated areas. Figure 13 gives differences in ten-day mean surface air pressure at 06:00 UTC between different groups of simulations. The SMOIS decrease shows to cause the decrease of the surface pressure, and the area with surface pressure decrease is consistent with the area of the SAT06 rise (Fig. 13a–d vs. Fig. 3g–j). The SMOIS-induced surface pressure drop is consistent with the above decrease of the 850 hPa geopotential height.

In previous studies of soil moisture sensitivity experiments over North America using different climate models, Oglesby and Erickson (1989) and Pal and Eltahir (2003) found a heat low at the surface and an enhanced positive height anomaly in the upper atmosphere because of reduced soil moisture, and Fischer et al. (2007) conducted sensitivity experiments for the 2003 European heat wave, also indicated a weak surface heat low and enhanced ridging in the mid-troposphere due to reduced soil moisture, and suggested a positive feedback mechanism between soil moisture, continental-scale circulation, and temperature. However, our results indicate a negative soil moisture-induced feedback mechanism between atmospheric circulation and temperature in the lower atmosphere, in addition to a positive feedback in the mid-troposphere. In fact, the low-level temperature is increased due to the SMOIS decrease, then the air volume expands after being heated and causes vertical and horizontal "movements", i.e., vertically, the secondary "circulation", whose direction is opposite to the actual airflow in the lower layer of the western Pacific subtropical high, actually results in the weakened downward low-level movement in the subtropical high; along with the horizontally expanded air that causes mass divergence in the lower layer, the pressure in the lower atmosphere is thus reduced under the constraint of the hydrostatic balance. Meanwhile, the expanded air induced by the SMOIS decrease lifts the pressure levels in the mid- and upper troposphere, e.g., the 500 hPa geopotential height is enhanced (Fig. 11). The difference in the feedback mechanism between Fischer et al. (2007) and our study is largely due to the fact that over East China, rather than a heat low, the dynamical subtropical high strongly persists in the lower atmosphere in addition to

ACPD
14, 11665–11714, 2014

the upper atmosphere, as is similar to the sensitivity study of Zeng et al. (2011) using different land surface schemes.

3.2.4 Physical processes: further quantitative analysis

As addressed in Sect. 2.3, due to few 2 m model outputs, all the terms for the physical processes in Eq. (2) can not be calculated directly. Simulation results show that the variation of the air temperature (T_{z1}) at the lowest model level (i.e., ∼ 30 m above ground where adequate simulation results are output, rather than the 2 m level) is basically consistent with that of air temperature at 2 m (i.e., SAT) in the simulations (e.g., shown in Fig. 14 for CTL), e.g., both temperatures gradually decrease with time in the afternoon with the lowest values occurring around 21:00–22:00 UTC, then rapidly rise and amount to the maximum values around 06:00 UTC. The consistency in the variations demonstrates that in the near-surface layer, the mechanism influencing 2 m SAT is similar to that influencing T_{z1}. Therefore, in this study, the advection, convection and diabatic terms in Eq. (2) are computed for the lowest model level to examine the relative importance of the terms influencing T_{z1}. In the same way, the explanation of the mechanism for the SMOIS-induced SAT changes can be given.

Table 2 lists area-averaged ten-day mean integral results of the four terms in Eq. (2) for nighttime and daytime, respectively. Although the temperature advection effect (ADV) might be relatively strong on the single-station temperature during some periods, the area-averaged ADV values, as one of the contributors to the T_{z1} change, show to be so small that they can be ignored in the 24 h simulations. For the convection effect term, under different soil moisture conditions the CON values show to be generally little changed, especially during daytime, with an exception for the DRY cases during nighttime, which leads to an overall warming effect as SMOIS is decreased (e.g., compared with CTL, DRY25 gives a 0.16 °C higher value for the CON term). Comparison of the CON term during daytime with that during nighttime indicates that the adiabatic temperature-rising effect of downward airflow in the western Pacific subtropical high at night is much stronger than that in the daytime (e.g., DRY25-CON temperature rises of 11.12 and 1.01 °C for nighttime and daytime, respectively), suggesting a much more significant influence on temperature change in the surface layer by regional atmospheric circulation at night. The difference in the heating effect is mainly due to the stratification difference between daytime and nighttime in the subtropical high, i.e., the daytime boundary layer is relatively well mixed compared to nighttime, and downward airflow has higher heating influence on the hydrostatically stable lower atmosphere during nighttime than during daytime. In addition, because the nighttime convection effect is more affected by the SMOIS change than the nearly unchanged daytime convection effect, relative to the WET conditions, an enhanced temperature rising is induced under the DRY conditions at the end of the 24 h-long integrations (Table 2).

Compared with absolute CON values for nighttime or daytime, corresponding absolute Q_t values are larger, i.e., the former are about two thirds of the latter at night and less than one fourth of that in the daytime (Table 2), indicating the dominant role of diabatic processes over the role of the convection process. During nighttime with the occurrence of boundary-layer temperature inversion induced by the longwave radiation cooling at the land surface, turbulence-induced diabatic cooling effect is larger than the adiabatic temperature rising effect, and therefore, the surface air becomes colder. During daytime with changed stratifications, diabatic heating dominants, and is much stronger than downward airflow-induced adiabatic temperature rising which is by far weaker than it is during nighttime. Very interestingly, although the diabatic effect dominates over the convection effect during nighttime and daytime, respectively (e.g., a nighttime value of −15.33 °C (11.01 °C), and a daytime value of 4.21 °C (0.99 °C) for the WET25 Q_t (CON) term), due to the opposite signs of the Q_t term during the different time periods, overall the diabatic effect does not dominate over the convection effect for the 24 h simulations; it is found that the diabatic (convection) effect is stronger than the convection (diabatic) in the CTL and WET (DRY) cases over the 24 h, e.g., WET25 (DRY25) gives the values of 12.05 and −12.76 °C (12.20 and −11.37 °C) for the 24 h CON and Q_t terms, respectively. Contrary to the CON consistent heating effect, the Q_t term has an overall effect of cooling. However, it should be noted that the overall

ACPD
14, 11665–11714, 2014

temperature rise, in response to the SMOIS decrease (e.g., the increase of the 24 h T_t term compared to CTL), is mainly because of the decreased cooling effect by the Q_t term instead of the increased heating effect by the CON term, e.g., for the 24 h integrations, the T_t term is changed from −0.14 °C (CTL) to 0.83 °C (DRY25), and the change is accompanied by a difference in the CON term (from 12.04 to 12.20 °C) and a much larger difference in the Q_t term (from −12.18 to −11.37 °C), which demonstrates that the overall diabatic processes is affected much more strongly by the SMOIS change. A closer comparison shows that this sensitivity is higher under the DRY conditions (Table 2), as is consistent with the sensitivity conclusion for SAT06 in Sect. 3.

In the 12 day simulations of warm-season convection, Trier et al. (2008) suggested that the initial soil moisture had an important influence on the thermodynamic variable, especially in the period when the ground heating is the strongest at daytime and its following period. Our results confirm this issue, and additionally show that the SMOIS-induced change in the nighttime cooling can exceed half of the change in the daytime heating in the high-temperature simulations (e.g., as CTL changed to DRY25, the Q_t term is decreased by 0.30 °C during nighttime, and increased by 0.57 °C during daytime, respectively; Table 2).

Similarly, the convection and diabatic processes play important roles in modifying the 2 m air temperature (SAT) change, in which the diabatic processes dominate over the adiabatic convection in the subtropical high. Additionally, the diabatic effect on the SAT variation is affected more strongly by the soil moisture change, e.g., with the SMOIS decrease, the SAT tends to be increased, mainly by the decreased cooling effect of the diabatic processes in the 24 h integrations. Because of the dry climate background in East China in late July 2003, sensible heat flux plays a dominant role in modifying the SAT among the low-level diabatic processes such as sensible and latent heating and radiation processes. Therefore, it suggests that primarily through modifying surface sensible heat flux, the initial soil moisture affects the simulation of occurrence of the East China extreme hot temperatures in late July 2003.

ACPD
14, 11665–11714, 2014

4 Summary and conclusions

Unlike research with a lot of attention paid to heat wave events at climate time scales, this paper intends to focus on the sensitivity of simulated high-temperature weather induced by different initial soil moisture in the 24 h short range. We adopt the Noah land surface scheme in the WRF model, Version 3 and design fifty 24 h integrations for the East China extremely hot event in late July 2003, with the initial soil moisture (SMOIS) changed, relative to the control run (CTL) by −25, −50, +25 and +50 % (i.e., the DRY25, DRY50, WET25, and WET50 simulations, respectively).

As a standard of high-temperature events in China, the above-35 °C surface air temperature (SAT) is used for preliminary analysis. SAT in East China roughly reaches the maximum value at 06:00 UTC (12:00 LT), and therefore we focus on SAT06, the 06:00 UTC SAT. Ten-day mean results indicate that CTL can generally reproduce the high temperature event. However, it is also found that the simulated event is sensitive to the change in initial soil moisture. With the SMOIS decrease, the central position of high SAT06 values is little changed, while the maximum SAT06 change shows to occur mainly over areas with above-35 °C temperature, which is accompanied by enlarged areas and intensification for simulated above-38 °C harmful high temperature. Compared with CTL, DRY25 results in a 1 °C SAT06 rising in general over inland surface of East China, while the DRY50 SAT06 rises more than 2 °C over most of the land, with a maximum value about 4 °C. Meanwhile, the high temperature simulations are found to be more sensitive to the decrease of SMOIS than the increase and SAT06 exhibits a nonlinear variation with the SMOIS change, e.g., the WET25 − WET50, CTL − WET25, DRY25 − CTL and DRY50 − DRY25 differences in SAT06 amount to 0.44, 0.73, 0.92 and 1.48 °C, respectively. These results are different from Fischer et al. (2007) who suggested that the simulated temperture is little sensitive to the further decrease of soil moisture (i.e., from −25 to −50 %), largely because simulated soil moisture generally does not approach the wilting point of vegetation within 24 h of integration while it

ACPD
14, 11665–11714, 2014

might do in hot climate simulations. Therefore, this study presents a stronger sensitivity for simulated hot weather at the short-range scale than at climate scales.

In terms of the mechanism influencing the extreme high SAT06, the SMOIS change results in changes in surface fluxes and atmospheric circulation, which play different roles in modifying SAT06. Sensible heat fluxes show to directly heat the lower atmosphere, present consistent patterns of difference fields with those of SAT06, suggesting that the SMOIS-induced sensible heat flux change is the most significant factor for the SAT06 change. This result is consistent with previous investigations which emphasize the influence of sensible heat flux on air temperature in weather simulations (e.g., Xue et al., 2001; Zeng et al., 2011), as well as in climate simulations (e.g., Fischer et al., 2007; Zhang et al., 2011).

SMOIS-induced latent heat flux change also shows to play a role in partitioning net radiation and therefore modifying the SAT06. Lower soil moisture can reduce evaporation (or latent heat flux) and the land cooling so that land surface temperature can be increased more easily, and therefore downward long wave radiation and sensible heat flux can also be increased, which is in favor of heating the lower atmosphere. The SMOIS increase is found to lead to the partitioning difference between sensible heat and latent heat fluxes, in a manner that the increase magnitude of latent heat flux is larger than the decrease magnitude of sensible heat flux. Moreover, with the increase of latent heat (evaporation), greenhouse effect induced by water vapor is reinforced, resulting in an enhancement of the surface net radiation, e.g., with the SMOIS increase of 25 % from DRY25 to CTL, the ten-day-mean surface net radiation is increased by $5\,\mathrm{W\,m^{-2}}$.

Overall, there exists a SMOIS-induced negative feedback in the lower layer between low-level temperature and circulation and a positive feedback in the mid-troposphere, i.e., low-level SAT rising (lowering), as induced by the SMOIS decrease (increase), results in geopotential-height lowering (rising) and leads to the weakening (strengthening) of the western Pacific subtropical high in the lower atmosphere; while in the mid-troposphere, the SMOIS decrease (increase), accompanied by temperature rising

ACPD
14, 11665–11714, 2014

(lowering), causes the geopotential-height increase (decrease), strengthening (weakening) the subtropical high. This feedback mechanism of temperature and circulation is different from that of Fischer et al. (2007) who used a regional climate model to simulate soil moisture-induced effects of the 2003 European heat wave at the seasonal scale, which is due to the differences between the synoptic systems controlling the high-temperature events.

Finally, we adopt the analogous relationship between the variation of the air temperature at the lowest model level (T_{z1}) and that of 2 m air temperature (SAT) to make a mechanism explanation for the processes through which initial soil moisture influences simulated SAT. Results from the air temperature equation for T_{z1} suggest that the diabatic processes dominates over the adiabatic convection for the SAT change in the WET and CTL simulations and are affected more strongly by the SMOIS change in the five groups of simulations, i.e., the contribution of the diabatic processes, which is dominated by sensible heat flux under the dry climate background, is changed by quite large amplitudes because of the SMOIS change, while only during nighttime under the DRY conditions the contribution of convection, which is caused by downward airflow and adiabatically heats the air in the subtropical high, show to be affected by the SMOIS change. Although the diabatic processes show opposite effects during different time periods (i.e., heating and cooling during daytime and nighttime, respectively), they are found to have an overall cooling effect on the SAT in the 24 h simulations, as is suggested to be mainly induced by sensible heat flux. Interestingly, although the adiabatic processes dominate over the convection process during daytime and during nighttime, respectively, they do not show to necessarily dominate during the 24 h-long periods. It is also found that as the SMOIS decreased, the SAT06 is increased, which is largely because of the reduced cooling effect of the diabatic processes, rather than the temperature-rising effect of convection. All these suggest that primarily by modifying surface sensible heat flux, the initial soil moisture has a substantial effect on the simulation of the extreme East China high-temperature weather event.

ACPD
14, 11665–11714, 2014

Additionally, we should note that this sensitivity study is implemented using the regional weather model. Because regional models are affected by initial and boundary conditions, as well as various model setups (such as domain size, areal location, spatial resolution and main physical options), the simulation performance of the model might be varied due to the differences in data and model configurations, and correspondingly, the simulation sensitivity might show some differences. For follow-up studies, using more cases and adopting more suites of model settings to explore the influence soil moisture would help us better understand the issue of soil moisture-induced sensitivity of hot temperature/heat wave events.

Acknowledgements. The authors would like to thank Dr. W. Lu and two anonymous reviewers for their helpful comments on the manuscript. This work was supported by the National Natural Science Foundation of China (Grant nos. 41275012 and 41205073).

References

Baldocchi, D., Falge, E., Gu, L., Olson, R., Hollinger, D., Running, S., Anthoni, P., Bernhofer, C., Davis, K., Evans, R., Fuentes, J., Goldstein, A., Katul, G., Law, B., Lee, X., Malhi, Y., Meyers, T., Munger, W., Oechel, W., Paw U, K. T., Pilegaard, K., Schmid, H. P., Valentini, R., Verma, S., Vesala, T., Wilson, K., and Wofsy, S.: FLUXNET: a new tool to study the temporal and spatial variability of ecosystem–scale carbon dioxide, water vapor, and energy flux densities, B. Am. Meteorol. Soc., 82, 2415–2434, 2001.

Barriopedro, D., Fischer, E. M., Luterbacher, J., Trigol, R. M., and Garcia-Herrerad, R.: The hot summer of 2010: redrawing the temperature record map of Europe, Science, 332, 220–224, doi:10.1126/science.1201224, 2011.

Beljaars, A. C. M., Viterbo, P., Miller, M. J., and Betts, A. K.: The anomalous rainfall over the United States during July 1993: sensitivity to land surface parameterization and soil moisture, Mon. Weather Rev., 124, 362–383, 1996.

Chen, F. and Dudhia, J.: Coupling an advanced land-surface hydrology model with the Penn State-NCAR MM5 modeling system. Part I: Model description and implementation, Mon. Weather. Rev., 129, 569–585, 2001.

ACPD

14, 11665–11714, 2014

Chou, M. D. and Suarez, M. J.: An Efficient Thermal Infrared Radiation Parameterization for Use in General Circulation Models, NASA Tech. Memo., 104606, 3, 85 pp., 1994.

Dickinson, R. E. and Kennedy, P.: Impacts on regional climate of Amazon deforestation, Geophys. Res. Lett., 19, 1947–1950, 1992.

Donat, M. G., Alexander, L. V., Yang, H., Durre, I., Vose, R., and Caesar, J.: Global land-based datasets for monitoring climatic extreme, B. Am. Meteorol. Soc., 94, 997–1006, 2013.

Douville, H.: Relative contribution of soil moisture and snow mass to seasonal climate predictability: a pilot study, Clim. Dynam., 34, 797–818, 2010.

Ek, M. B., Mitchell, K. E., Lin, Y., Rogers, E., Grunmann, P., Koren, V., Gayno, G., and Tarpley, J. D.: Implementation of Noah land surface model advances in the National Centers for Environmental Prediction operational Mesoscale Eta Model, J. Geophys. Res., 108, 8851, doi:10.1029/2002JD003296, 2003.

Fennessy, M. J. and Kinter, J. L.: Climatic feedbacks during the 2003 European heat wave, J. Climate, 24, 5953–5967, 2011.

Fennessy, M. J. and Shukla, J.: Impact of initial soil wetness on seasonal atmospheric prediction, J. Climate, 12, 3167–3180, 1999.

Ferranti, L. and Viterbo, P.: The European summer of 2003: Sensitivity to soil water initial conditions, J. Climate, 19, 3659–3680, 2006.

Fischer, E. M., Seneviratne, S. I., Vidale, P. L., Lüthi, D., and Schär, C.: Soil moisture–atmosphere interactions during the 2003 European summer heat wave, J. Climate, 20, 5081–5099, 2007.

Guo, Z., Dirmeyer, P. A., and DelSole, T.: Land surface impacts on subseasonal and seasonal predictability, Geophys. Res. Lett., 38, L24812, doi:10.1029/2011GL049945, 2011.

Guo, Z., Dirmeyer, P. A., DelSole, T., and Koster, R. D.: Rebound in atmospheric predictability and the role of the land surface, J. Climate, 25, 4744–4749, 2012.

Hirschi, M., Seneviratne, S. I., Alexandrov, V., Boberg, F., Boroneant, C., Christensen, O. B., Formayer, H., Orlowsky, B., and Stepanek, P.: Observational evidence for soil-moisture impact on hot extremes in southeastern Europe, Nat. Geosci., 4, 17–21, 2011.

Holt, T., Niyogi, D., Chen, F., LeMone, M. A., Manning, K., and Qureshi, A. L.: Effect of land-atmosphere interactions on the IHOP 24–25 May 2002 convection case, Mon. Weather Rev., 134, 113–133, 2006.

Hong, S.-Y., and Pan, H.-L.: Nonlocal boundary layer vertical diffusion in a medium-range forecast model, Mon. Weather Rev., 124, 2322–2339, 1996.

Hong, S.-Y., Noh, Y., and Dudhia, J.: A new vertical diffusion package with an explicit treatment of entrainment processes, Mon. Weather Rev., 134, 2318–2341, doi:10.1175/MWR3199.1, 2006.

Janjiæ, Z. I.: The step-mountain Eta coordinate model: further developments of the convection, viscous sub-layer and turbulence closure schemes, Mon. Weather Rev., 122, 927–945, 1994.

Kalkstein, L. S., Jamason, P. F., Greene, J. S., Libby, J., and Robinson, L.: The Philadelphia hot weather-health watch/warning system: development and application, summer 1995, B. Am. Meteorol. Soc., 77, 1519–1528, 1996.

Koster, R. D., Dirmeyer, P. A., Guo, Z., Bonan, G., Chan, E., Cox, P., Gordon, C. T., Kanae, S., Kowalczyk, E., Lawrence, D., Liu, P., Lu. C. H., Malyshev, S., McAvaney, B., Mitchell, K., Mocko, D., Oki, T., Oleson, K., Pitman, A., Sud, Y. C., Taylor, C. M., Verseghy, D., Vasic, R., Xue, Y., and Yamada, T.: Regions of strong coupling between soil moisture and precipitation, Science, 305, 1138–1141, 2004.

Koster, R. D., Sud, Y. C., Guo, Z., Dirmeyer, P. A., Bonan, G., Oleson, K. W., Chan, E., Verseghy, D., Cox, P., Davies, H., Kowalczyk, E., Gordon, C. T., Kanae, S., Lawrence, D., Liu, P., Mocko, D., Lu, C.-H., Mitchell, K, Malyshev, S., McAvaney, B., Oki, T., Yamada, T., Pitman, A., Taylor, C. M., Vasic, R., and Xue, Y.: GLACE: the Global Land–Atmosphere Coupling Experiment. Part I: Overview, J. Hydrometeorol., 7, 590–610, 2006.

Larsen, J.: Record Heat Wave in Europe Takes 35000 Lives, Earth Policy Institute, p. 1, 2003.

Lau, W. K. M. and Kim, K.-M.: The 2010 Pakistan flood and Russian heat wave: teleconnection of hydrometeorological extremes, J. Hydrometeorol., 13, 392–403, 2012.

Lei, M., Niyogi, D., Kishtawal, C., Pielke Sr., R. A., Beltrán-Przekurat, A., Nobis, T. E., and Vaidya, S. S.: Effect of explicit urban land surface representation on the simulation of the 26 July 2005 heavy rain event over Mumbai, India, Atmos. Chem. Phys., 8, 5975–5995, doi:10.5194/acp-8-5975-2008, 2008.

Lin, J., Bi, B. G., and He, J. H.: Physical mechanism responsible for western Pacific subtropical high variation and hot wave in southern China in July 2003, Chinese J. Atmos. Sci., 29, 594–599, 2005 (in Chinese).

Lin, Y.-L., Farley, R. D., and Orville, H. D.: Bulk parameterization of the snow field in a cloud model, J. Clim. Appl. Meteorol., 22, 1065–1092, 1983.

ACPD
14, 11665–11714, 2014

Sensitivity of high-temperature weather to initial soil moisture

X.-M. Zeng et al.

Liu, H., Blanken, P. D., Weidinger, T., Nordbo, A., and Vesala, T.: Variability in cold front activities modulating cool-season evaporation from a southern inland water in the USA, Environ. Res. Lett., 6, 024022, doi:10.1088/1748-9326/6/2/024022, 2011.

Lyon, B. and Dole, R. M.: A diagnostic comparison of the 1980 and 1988 US summer heat wave-droughts, J. Climate, 8, 1658–1675, 1995.

Mlawer, E. J., Taubman, S. J., Brown, P. D., Iacono, M. J., and Clough, S. A.: Radiative transfer for inhomogeneous atmosphere: RRTM, a validated correlated-*k* model for the long-wave, J. Geophys. Res., 102, 16663–16682, doi:10.1029/97JD00237, 1997.

Oglesby, R. J. and Erickson, D.: Soil moisture and the persistence of North American drought, J. Climate, 2, 1362–1380, 1989.

Pal, J. S. and Eltahir, E. A. B.: A feedback mechanism between soil moisture distribution and storm tracks, Q. J. Roy. Meteor. Soc., 129, 2279–2297, 2003.

Pielke, R. A.: Influence of the spatial distribution of vegetation and soils on the prediction of cumulus convective rainfall, Rev. Geophys., 39, 151–177, 2001.

Seneviratne, S. I., Koster, R. D., Guo, Z., Dirmeyer, P. A., Kowalczyk, E., Lawrence, D., Liu, P., Lu, C.-H., Mocko, D., Oleson, K. W., and Verseghy, D.: Soil moisture memory in AGCM simulations: analysis of Global Land-Atmosphere Coupling Experiment (GLACE) data, J. Hydrometeorol., 7, 1090–1112, 2006.

Shukla, J. and Mintz, Y.: Influence of the land-surface evapotransporation on the Earth's climate, Science, 215, 1498–1500, 1982.

Skamarock, W. C., Klemp, J., Dudhia, J., Gill, D. O., Barker, D. M., Duda, M. G., Huang, X. Y., Wang, W., and Powers, J. G.: A Description of the Advanced Research WRF Version 3, NCAR Technical note NCARTN-475+STR, Natl. Cent. for Atmos. Res., Boulder, CO, USA, 113 pp., 2008.

Stefanon, M., D'Andrea, F., and Drobinski, P.: Heatwave classification over Europe and the Mediterranean region, Environ. Res. Lett. 7, 014023, doi:10.1088/1748-9326/7/1/014023, 2012.

Sun, J., Trier, S. B., Xiao, Q., Weisman, M. L., Wang, H., Ying, Z., Xu, M., and Zhang, Y.: Sensitivity of 0–12-h warm-season precipitation forecasts over the central United States to model initialization, Weather Forecast., 27, 832–855, 2012.

Tan, J., Zheng, Y., and Song, G.: Heat wave impacts on mortality in Shanghai, 1998 and 2003, Int. J. Biometeorol., 51, 193–200, 2007.

ACPD

14, 11665–11714, 2014

Sensitivity of high-temperature weather to initial soil moisture

X.-M. Zeng et al.

Trier, S. B., Chen, F., and Manning, K. W.: Sensitivity of the PBL and precipitation in 12-day simulations of warm-season convection using different land surface model and soil wetness conditions, Mon. Weather Rev., 136, 2321–2343, 2008.

Viterbo, P. and Betts, A. K.: Impact of the ECMWF reanalysis soil water on forecasts of the July 1993 Mississippi flood, J. Geophys. Res., 19, 361–366, 1999.

Vinnikov, K. Y. and Yeserkepova, I. B.: Soil moisture: empirical data and model results, J. Climate, 4, 66–79, 1990.

Whitaker, J. S., Hamill, T. M., Wei, X., Song, Y., and Toth, Z.: Ensemble data assimilation with the NCEP Global Forecast System, Mon. Weather Rev., 136, 463–482, 2008.

Willmott, C. J., Matsuura, K., and Legates, D. L.: Global air temperature and precipitation: regridded monthly and annual climatologies (Version 2.01), available at: http://climate.geog.udel.edu/ (last access: 6 May 2014), 2013.

Wolfson, N., Atlas, R., and Sud, Y. C.: Numerical experiments related to the summer 1980 US heat wave, Mon. Weather Rev., 115, 1345–1357, 1987.

World Meteorological Organization: The Global Climate 2001–2010: a Decade of Climate Extremes – Summary Report, WMO-No. 1119, 2013.

Xue, Y., Zeng, F. J., Mitchell, K. E., Janjic, Z., and Rogers, E.: The impact of land surface processes on simulations of the US hydrological cycle: a case study of the 1993 flood using the SSiB land surface model in the NCEP Eta regional model, Mon. Weather Rev., 129, 2833–2860, 2001.

Yang, H. and Li, C. Y.: Diagnostic study of serious high temperature over South China in 2003 summer, Climatic and Environmental Research, 10, 81–85, 2005 (in Chinese).

Zeng, X.-M., Zhao, M., Su, B., Tang, J., Zheng, Y., Zhang, Y., and Chen, J.: Effects of the land-surface heterogeneities in temperature and moisture from the "combined approach" on regional climate: a sensitivity study, Global Planet. Change, 37, 247–263, 2003.

Zeng, X.-M., Wu, Z., Xiong, S., Song, S., Zheng, Y., and Liu, H.: Sensitivity of simulated short-range high-temperature weather to land surface schemes by WRF, Science China: Earth Sciences, 54, 581–590, doi:10.1007/s11430-011-4181-6, 2011.

Zhang, J. and Wu, L.: Land-atmosphere coupling amplifies hot extremes over China, Chinese Sci. Bull., 56, 3328–3332, doi:10.1007/s11434-011-4628-3, 2011.

Zhang, S., Zhang, D., Wang, S., and Song, Y.: Climatic characteristics of summer high temperature and assessment methods in the large cities of North China, J. Geogr. Sci., 16, 13–22, 2006.

ACPD
14, 11665–11714, 2014

Sensitivity of high-temperature weather to initial soil moisture

X.-M. Zeng et al.

Table 1. Ten-day means for 24 h-averaged and 06:00 UTC sensible heat flux (SHF; $W m^{-2}$), latent heat flux (LHF; $W m^{-2}$), LHF plus SHF, net radiation (RN; $W m^{-2}$), and surface air temperatures (SAT; °C) in the five groups of simulations.

	SHF		LHF		SHF + LHF		RN		SAT	
	24 h	06:00 UTC	24 h	06:00 UTC	24 h	06:00 UTC	24 h	06:00 UTC	24 h	06:00 UTC
DRY50	75.1	241.5	92.5	234.4	167.6	475.9	210.7	623.4	31.34	36.19
DRY25	45.8	159.2	133.3	340.4	179.1	499.7	220.8	646.9	30.68	34.75
CTL	31.4	119.3	154.7	393.8	186.1	513.1	226.0	658.7	30.21	33.79
WET25	21.3	91.7	170.8	432.1	192.1	523.8	230.1	666.8	29.81	33.06
WET50	15.8	76.8	180.1	452.3	195.9	529.1	232.2	670.3	29.57	32.62

ACPD
14, 11665–11714, 2014

Table 2. Area-averaged ten-day mean integral results of the four terms in the T_{z1} equation (i.e., Eq. 2) for the 24 h, nighttime (11:00–22:00 UTC) and daytime (22:00–06:00 UTC), respectively (unit: °C). Note that the daytime is separated into two parts by the nighttime in the 24 h integrations, and only one part is considered in the statistics, which is assumed to be reasonable and have little influence for the analysis.

	T_t			ADV			CON			Q_t		
	24 h	Nighttime	Daytime	24 h	Nighttime	Daytime	24 h	Nighttime	Daytime	24 h	Nighttime	Daytime
DRY50	2.22	−5.12	7.37	-2.6×10^{-05}	-1.2×10^{-05}	4.4×10^{-05}	12.60	11.42	1.01	−10.38	−16.54	6.34
DRY25	0.83	−4.70	6.24	6.2×10^{-05}	2.8×10^{-05}	1.6×10^{-05}	12.20	11.12	1.01	−11.37	−15.72	5.24
CTL	−0.14	−4.51	5.66	-1.8×10^{-05}	-4.9×10^{-06}	2.7×10^{-06}	12.04	10.91	0.98	−12.18	−15.42	4.67
WET25	−0.71	−4.32	5.20	-1.8×10^{-04}	3.0×10^{-05}	-2.1×10^{-04}	12.05	11.01	0.99	−12.76	−15.33	4.21
WET50	−1.20	−4.24	4.92	1.0×10^{-04}	1.2×10^{-04}	-3.0×10^{-05}	12.01	11.06	0.98	−13.21	−15.30	3.94

ACPD
14, 11665–11714, 2014

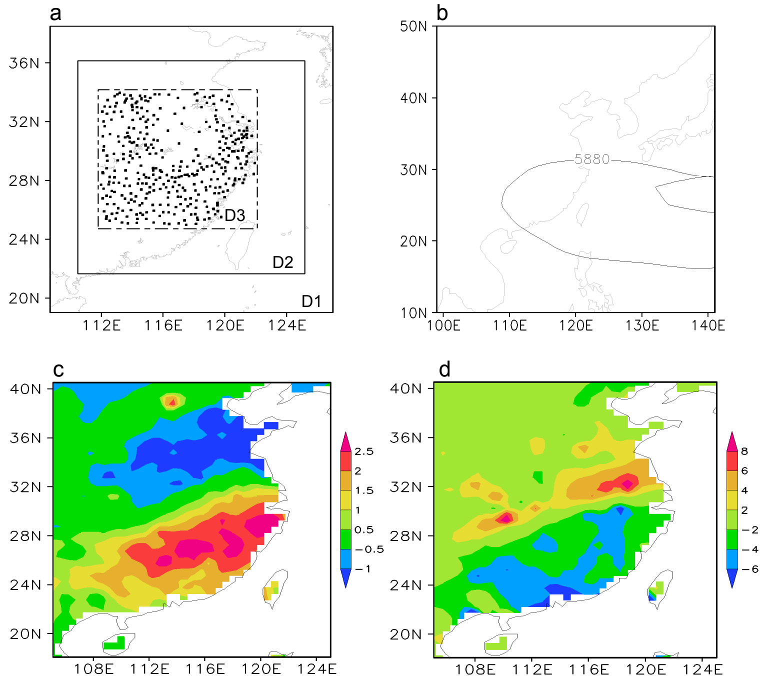

Fig. 1. The study areas and the climatology. **(a)** Model domain, where the D1 and D2 sub-areas are the large and nested areas, respectively, while D3 is the "core" region of southeastern China where the extreme hot temperatures occurred and meteorological stations are marked with dots for use in the assessment; **(b)** the 500 hPa 5880 gpm contours for July 2003 (solid line) and base period (1971–2000; dashed line) climatological averages; **(c)** July 2003 SAT anomaly, i.e., departures from the base period (1971–2000) average (unit: °C); **(d)** same as **(c)**, but for precipitation (unit: mm d^{-1}).

ACPD
14, 11665–11714, 2014

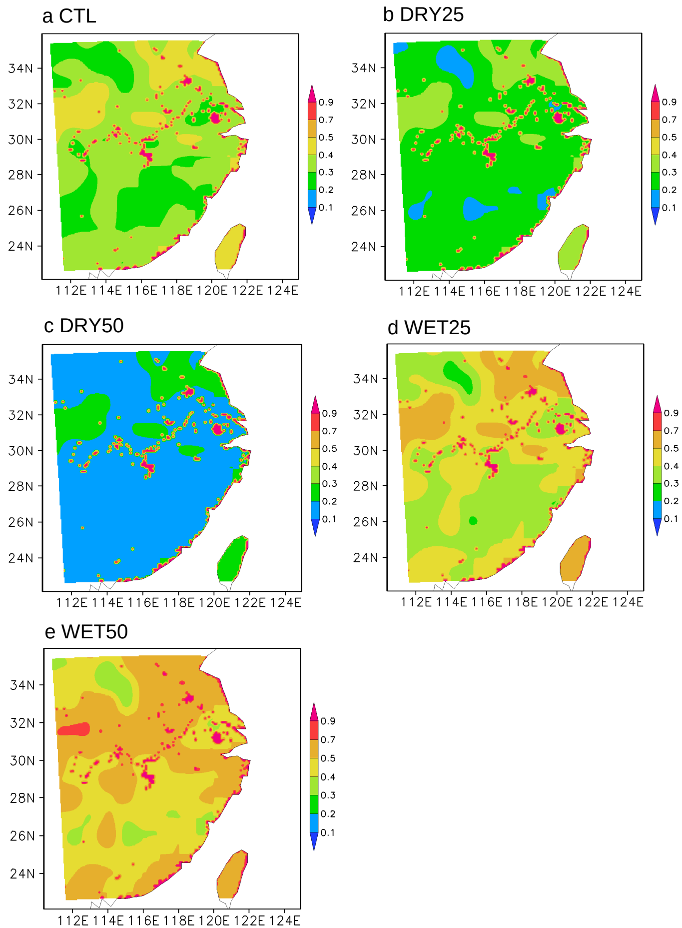

Fig. 2. Initial surface soil moisture fields at 06:00 UTC 20 July 2003 in the D21 simulations (unit: $m^3 m^{-3}$).

ACPD
14, 11665–11714, 2014

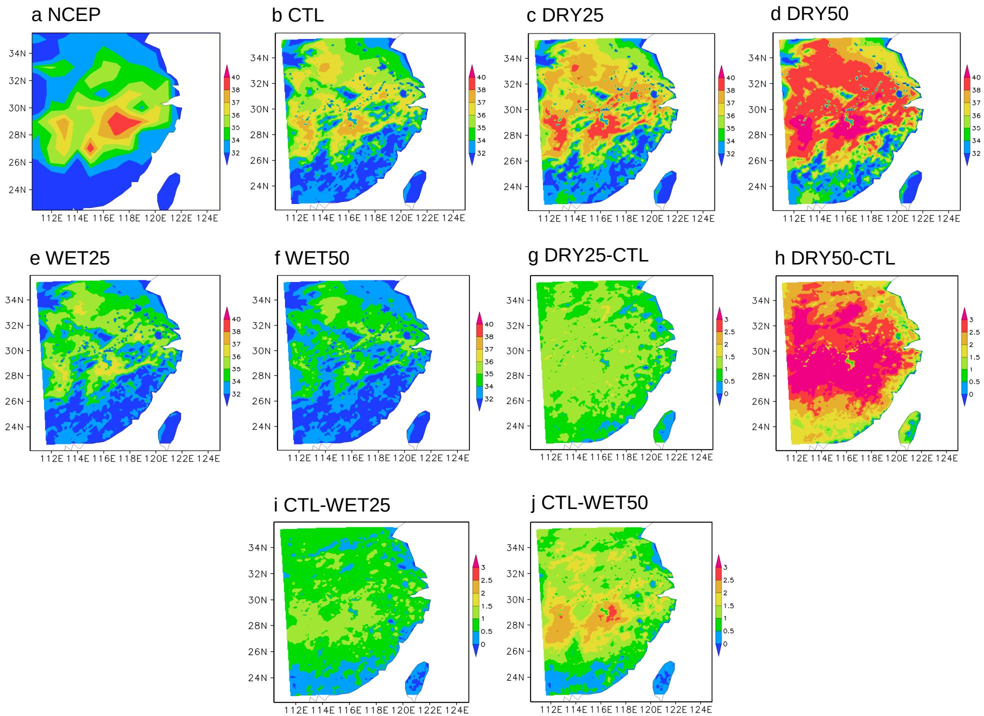

Fig. 3. Spatial distributions of ten-day mean SAT06 in the simulations (unit: °C).

ACPD
14, 11665–11714, 2014

Sensitivity of high-temperature weather to initial soil moisture

X.-M. Zeng et al.

ACPD
14, 11665–11714, 2014

Sensitivity of high-temperature weather to initial soil moisture

X.-M. Zeng et al.

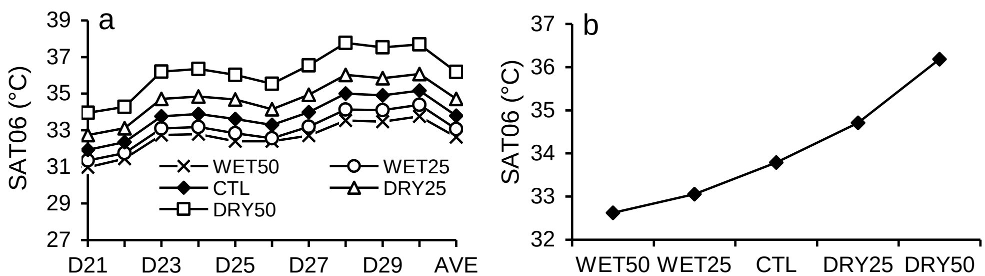

Fig. 4. Average SAT06 values for area D3 in the simulations. **(a)** Values as changed with individual simulations with an average (AVE) for each group of simulations; **(b)** ten-day means as changed with the five groups of simulations.

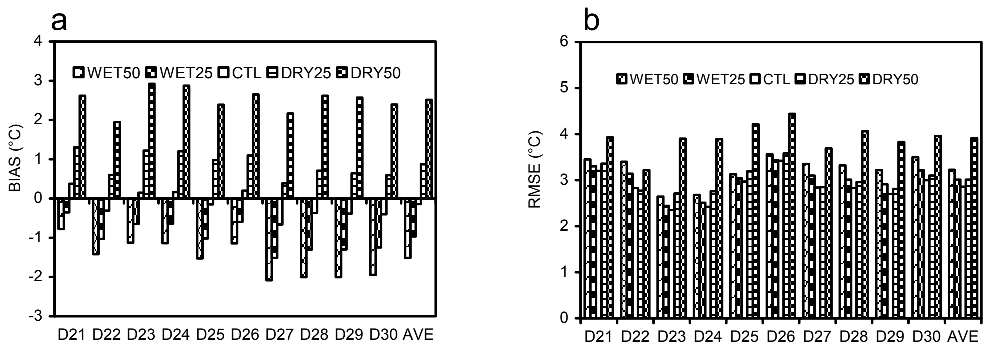

Fig. 5. BIAS **(a)** and RMSE **(b)** values for SAT06 in individual simulations with a ten-day average (AVE).

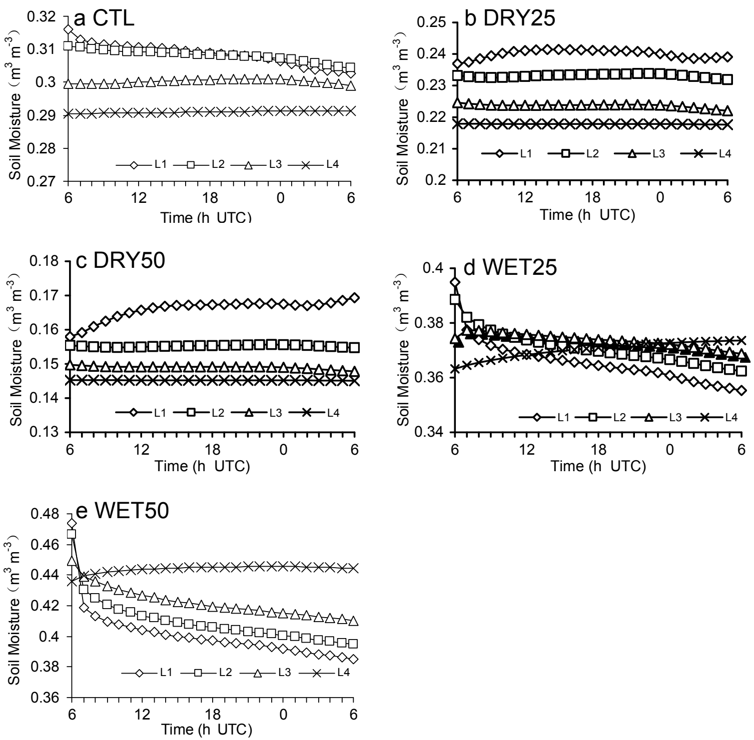

Fig. 6. Mean hourly variations of soil moisture (unit: $m^3\,m^{-3}$) in the five groups of 24 h-long simulations for 20–29 July 2003, where L1, L2, L3 and L4 represent 10, 30, 60 and 100 cm-thick soil layers, respectively.

ACPD
14, 11665–11714, 2014

Title Page
Abstract Introduction
Conclusions References
Tables Figures
◀ ▶
Back Close
Full Screen / Esc
Printer-friendly Version
Interactive Discussion

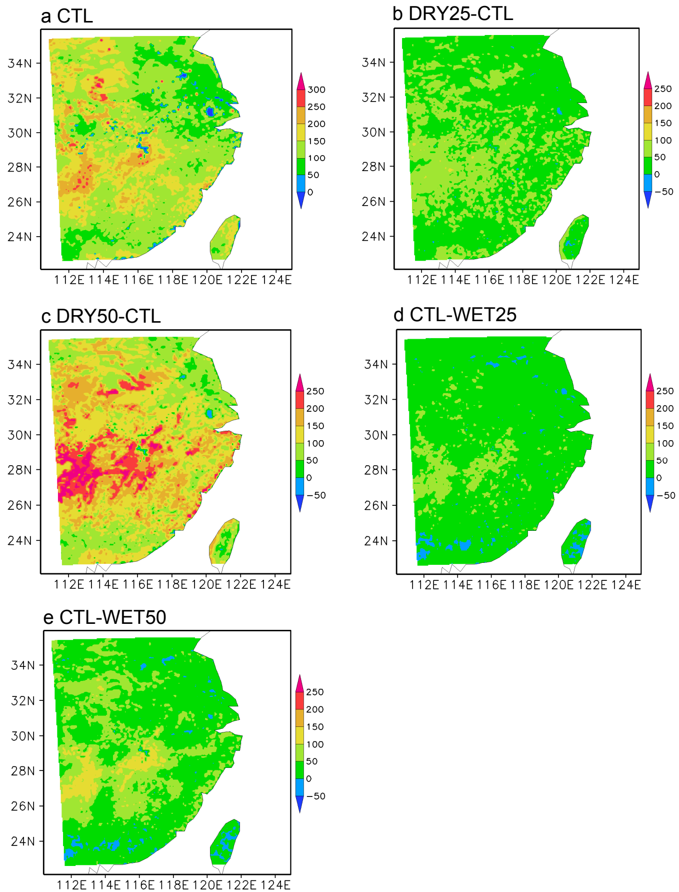

Fig. 7. Spatial distributions of the ten-day mean 06:00 UTC sensible heat fluxes in the simulations (unit: $W m^{-2}$).

ACPD
14, 11665–11714, 2014

Sensitivity of high-temperature weather to initial soil moisture

X.-M. Zeng et al.

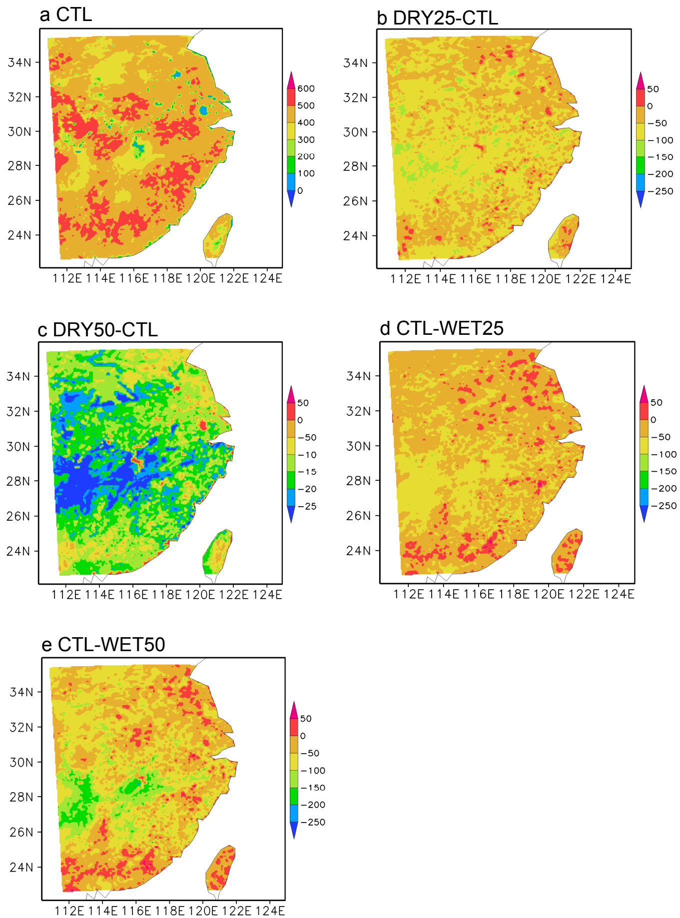

Fig. 8. As Fig. 7, but for latent heat fluxes.

ACPD
14, 11665–11714, 2014

Sensitivity of high-temperature weather to initial soil moisture

X.-M. Zeng et al.

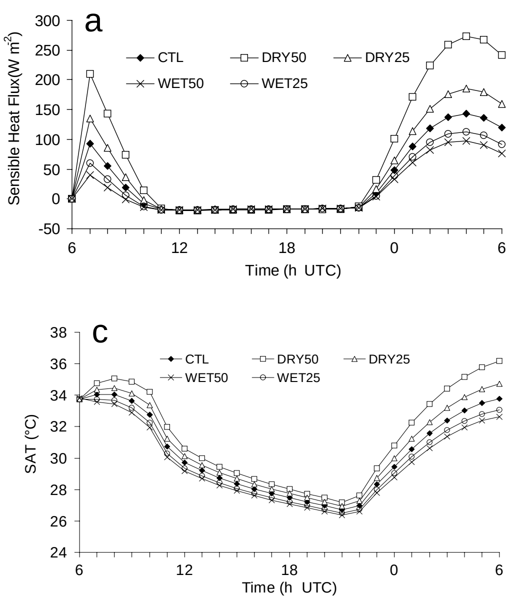

Fig. 9. Mean hourly variations of area-averaged (area D3) surface quantities in the five groups of simulations for 20–29 July 2003, where initial flux values are zero and initial temperatures have the same values. **(a)** Sensible heat flux; **(b)** latent heat flux; **(c)** SAT.

ACPD
14, 11665–11714, 2014

Sensitivity of high-temperature weather to initial soil moisture

X.-M. Zeng et al.

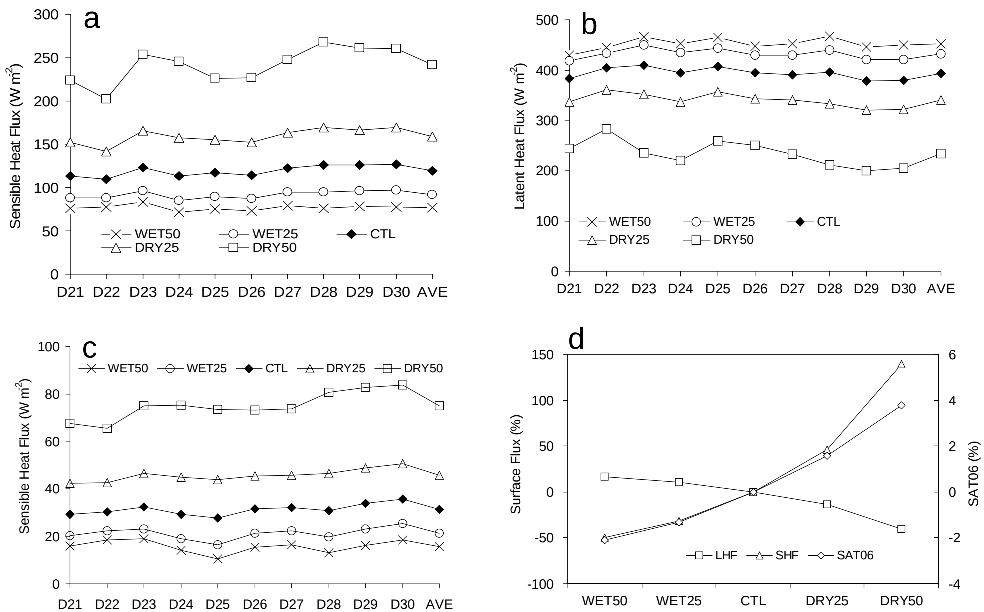

Fig. 10. Area-averaged sensible heat and latent heat fluxes and SAT06. **(a)** 06:00 UTC sensible heat flux in individual simulations with a ten-day average (AVE) for each group of simulations; **(b)** as **(a)**, but for latent heat flux; **(c)** as **(a)**, but for 24 h mean sensible heat flux (SHF); **(d)** relative differences (%) in ten-day mean 24 h-averaged sensible heat flux (SHF), latent heat flux (LHF) and SAT06, as compared to CTL.

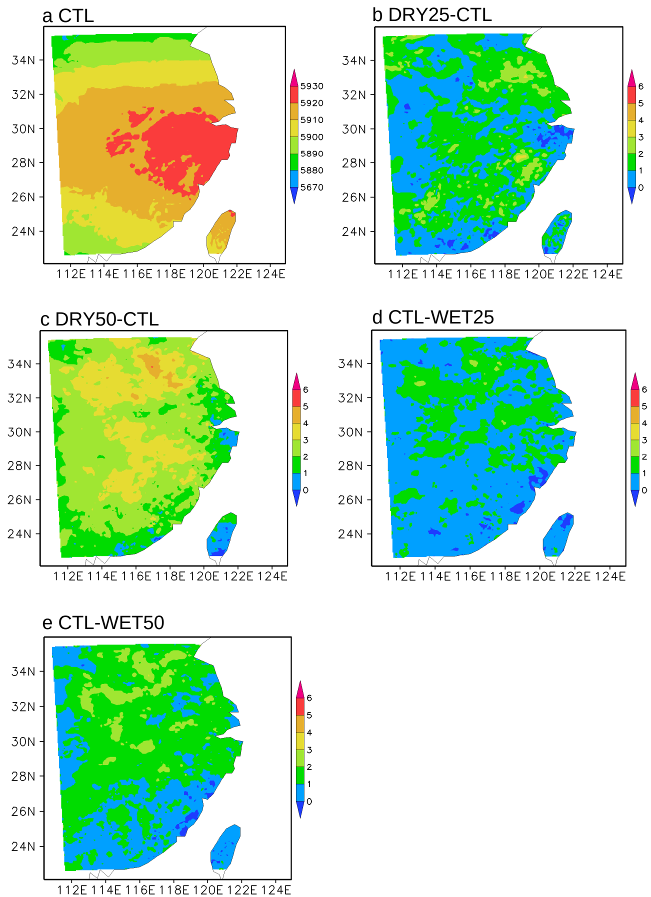

Fig. 11. Ten-day mean 06:00 UTC 500 hPa geopotential height fields and the soil moisture-induced differences in the five groups of simulations (unit: gpm).

ACPD
14, 11665–11714, 2014

Sensitivity of high-temperature weather to initial soil moisture

X.-M. Zeng et al.

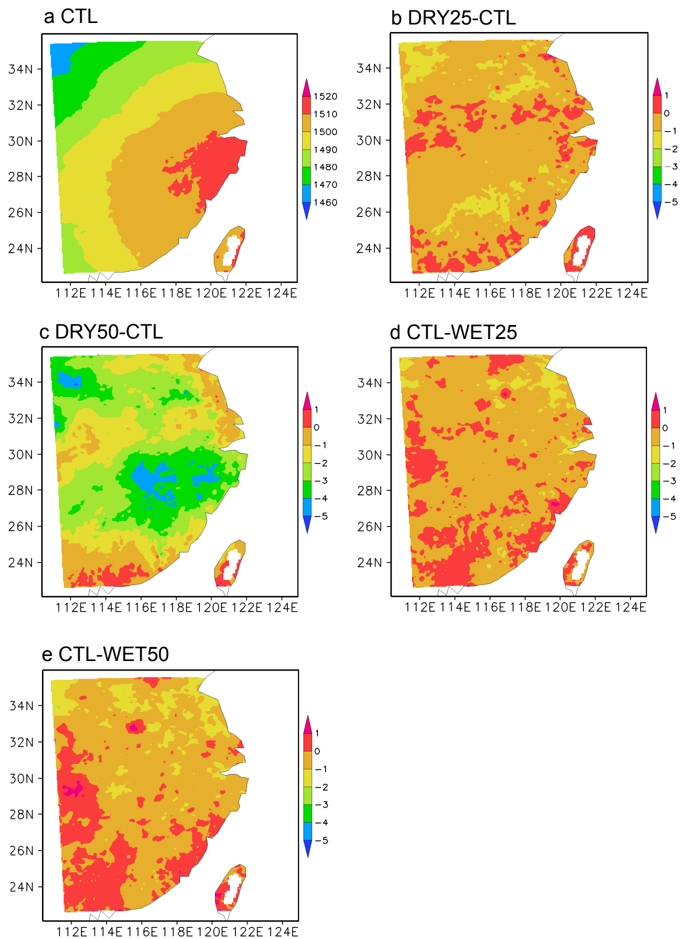

Fig. 12. Same as Fig. 11, but for 850 hPa.

ACPD
14, 11665–11714, 2014

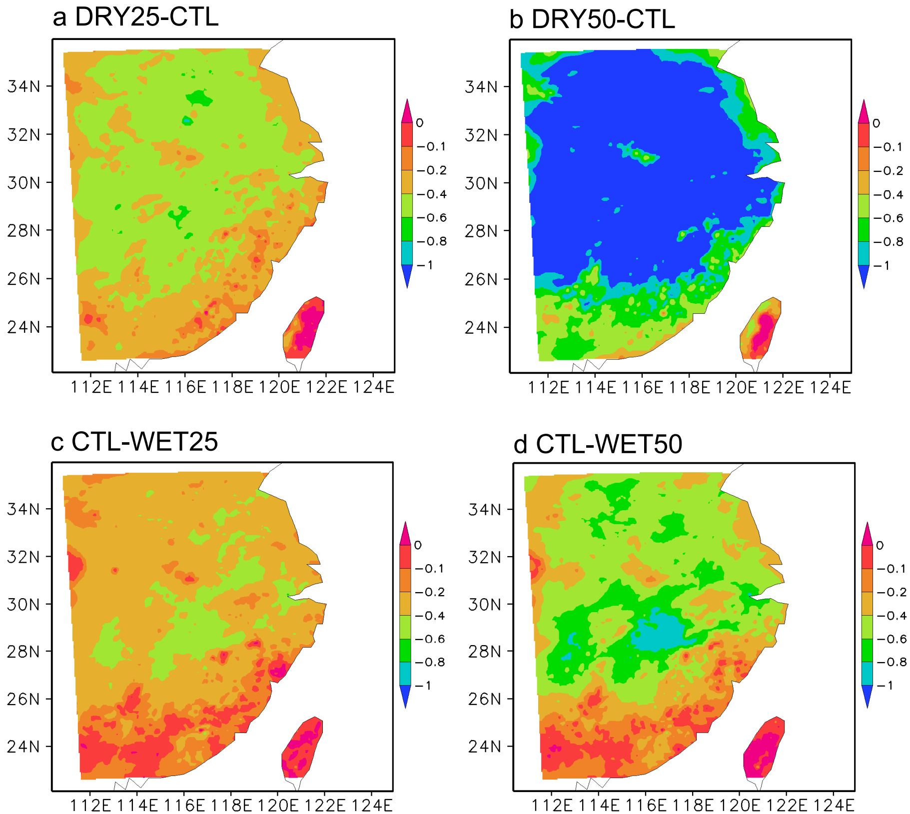

Fig. 13. Ten-day mean 06:00 UTC surface pressure difference fields as compared between different groups of simulations (unit: hPa).

ACPD
14, 11665–11714, 2014

Sensitivity of high-temperature weather to initial soil moisture

X.-M. Zeng et al.

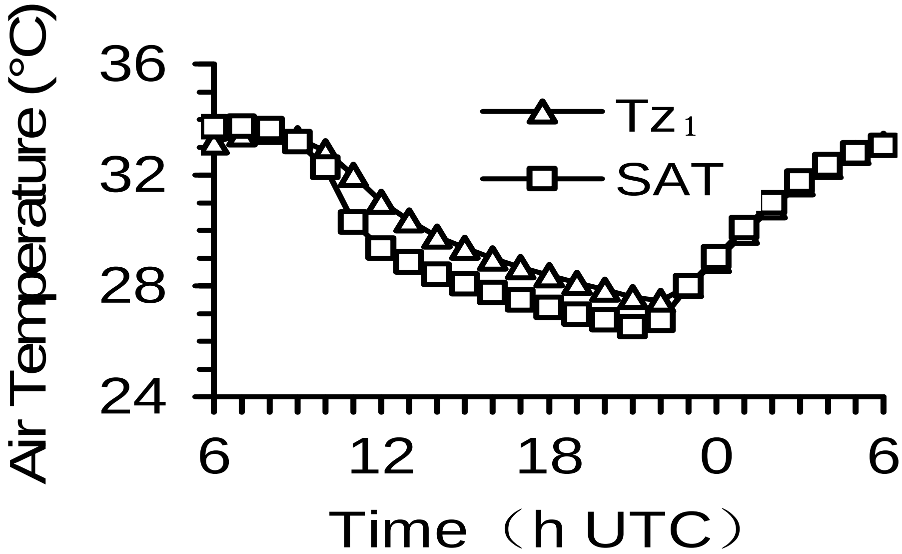

Fig. 14. Mean hourly variations of 2 m air temperature (SAT) and the air temperature at the lowest model level (T_{z1}) in the CTL run for 20–29 July 2003.

ACPD
14, 11665–11714, 2014

Sensitivity of high-temperature weather to initial soil moisture

X.-M. Zeng et al.